DOI: XXXXXXXXXXXXXXXXXXXX - ISSN: XXXX-XXXX - Vol 1(1), 2020, pp: XX:XX

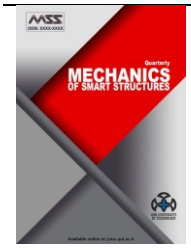

MECHANICS
OF SMART STRUCTURES
Available Online at: http://jmss.qut.ac.ir/

QOM UNIVERSITY OF TECHNOLOGY

# Three dimensional transient coupled thermoelasticity analysis of FGM cylindrical panel embedded in piezoelectric layers

**ARTICLE INFO**

***Article Type***
Original Research

***Authors***
A. Alibeigloo [1]
M. Talebitooti[2]

[1]Dept. of Mechanical Engineering, Faculty of Engineering, Tarbiat Modares University, Tehran, Iran, abeigloo@modares.ac.ir
[2]Dept. of Mechanical Engineering, Qom University of Technology, Qom, Iran, talebi@qut.ac.ir

**** Correspondence***
Dept. of Mechanical Engineering, Qom University of Technology, Khodakaram Boulevard,Qom, Iran. Postal Code: 71551313. talebi@qut.ac.ir

***Article History***
Received: november 09, 2020
Accepted: may 01, 2021
ePublished: June 13, 2021

**ABSTRACT**

Transient response of a simply supported functionally graded material (FGM) cylindrical panel integrated with sensor and actuator piezoelectric layers and subjected to electric field and thermal shock is investigated using generalized coupled thermoelasticity based on the Lord-Shulman theory. Thermoelastic material properties of the FGM are assumed to vary continuously along the radial direction according to simple power law with assumption of constant Poisson ratio. Applying Fourier series expansion along the axial and circumferential direction and state space technique along the radial coordinate to the constitutive equation and governing differential equation of motion result in state space matrix equations which are solved analytically by using Laplace transform. The inverse Laplace transform is used to obtain the solution in time domain. In parametric study effect of relaxation temperature constant, applied voltage and thermal shock on thermoelastic response of FGM cylindrical panel attached to piezoelectric sensor and actuator layers are studied. From parametric study it was concluded that the material inhomogeneity significantly affect coupled thermoelastic behavior of the hybrid FGM cylindrical panel.

**Keywords:** Functionally graded material; Cylindrical panels; Piezoelectric material; Thermal shock; State space.

# 1 Introduction

Functionally graded materials (FGM) are modern composite in which the composition of materials varies continuously as function of spatial coordinates which causes to achieve continuous and smooth variation of material properties. Usually FGM are made from combination of ceramic to provide high-temperature resistance due to its low thermal conductivity and metal to prevent fracture caused by stresses due to the high temperature gradient in a short time. Stresses in FGM structures subjected to mechanical or thermal loads can be optimized by selecting an appropriate material distribution. On the other hand, piezoelectric materials have coupled effects between the electric fields and the elastic deformation. It is possible to make a system of intelligent materials by combining these piezoelectric materials with FGMs.

New structures including FGM members bonded with piezoelectric actuators and sensors are smart in response to environmental changes. For example, thermal loading causes significant thermal stresses due to thermal gradient across the thickness and due to widely different thermal properties of the adjacent layers. Surface bonded piezoelectric layers reduce unwanted displacements and stresses caused by elevated or reduced temperature environment. Many studies on electromechanical and thermal response of smart structures are available in the literature. Based on three-dimensional piezothermoelasticity formulation, Ootao and Tanigawa [1] presented transient response of FGM rectangular plate bonded to a piezoelectric layer. Based on theory of elasticity, Cho and Kardomateas [2] used Hankel and Laplace transformation to investigate elastodynamic behavior of orthotropic cylindrical shell subjected to thermal shock. Based on first–order shear deformable plate theory (FSDPL), Liew et al. [3] presented a finite element formulation for active control of the shape and vibration of FGM plates integrated with actuator and sensor layer under thermal gradient. Axisymmetric dynamic thermoelastic analysis of a non-homogeneous orthotropic long cylindrical shell subjected to thermal shock was studied by Ding et al. [4]. Dai and Wang [5] presented an analytical method for stress wave propagation of spherically symmetric motion in laminated piezoelectric shells subjected to thermal shock and electric excitation loads by using finite Hankel transform and Laplace transform. Thermo-electro-elastic transient response of a piezoelectric hollow spherical shell and cylindrical shell subjected to arbitrary thermal shock was presented analytically by Dai and Wang [6] using Hankel transform and Laplace transform. Oh [7] used Hamilton's variational principles and finite element method to analysis of nonlinear dynamic of piezolaminated plates under thermo-electric load. Based on higher-order shear deformation plate theory and using general von Karman-type equation, Huang and Shen [8] presented dynamic response of FGM plates with surface-bonded piezoelectric layers in thermal environments. Giannopoulos and Vantomme [9] used finite element method to analysis dynamic behavior of composite plates integrated with piezoelectric layers under different thermal, mechanical and electrical loads. Li et al. [10] investigated bending behavior of a functionally graded, transversely isotropic, magneto–electro-elastic circular plate subjected to uniform load by using appropriate polynomials in the radial coordinate for the displacements and electric potential. Based on the classical plate theory, Ebrahimi and Rastgoo [11] investigated analytically free vibration behavior of thin circular FG plates integrated with two uniformly distributed actuator layers made of piezoelectric. Nonlinear vibration analysis of thin annular FG plate embedded in two piezoelectric layers was carried out analytically by Ebrahimi and Rastgoo [12] in the frame work of Kirchhoff plate theory. Based on Mindlin plate theory, Ebrahimi et al. [13] studied analytically free vibration of moderately

thick circular FG plate integrated with two thin piezoelectric layers in the framework on Mindlin plate theory. Thermo-elastic behavior of functionally graded orthotropic hollow sphere under thermal shock was studied by Kar and Kanoria [14] using linear theories of generalized thermo-elasticity and Laplace transform. Ebrahimi et al. [15] studied free vibration of moderately thick shear deformable annular functionally graded plate coupled with piezoelectric layers in the frame work of Mindlin's plate theory. Nonlinear vibration of piezoelectrically actuated circular FGM plates was studied by Ebrahimi et al. [16] based on Kirchhoff's-Love hypothesis with von-Karman type geometrical large nonlinear deformations. Alibeigloo [17] used Fourier series state space technique to analyze thermoelastic behavior of simply supported FGM rectangular plate embedded in piezoelectric layers. Two-dimensional elastodynamic transient behavior of finite simply supported cylindrical shell under nonuniform thermal shock was investigated by Ying and Wang [18] using uncoupled linear thermoelastic theory. Based on Lord and Shulman theory, Chitikireddy et al.[19] used Generalized thermoelastic theory proposed by Lord and Shulman to investigate dynamic thermoelastic behavior of the anisotropic infinite cylinder subjected to concentrated heating at the outer surface. Based on theory of elasticity, Alibeigloo [20] presented an exact solution of a FGM cylindrical panel embedded in piezoelectric layers under thermo-electro-mechanical loads. Ebrahimi [21] performed analytical study of a thermo-piezoelectrically actuated sandwich circular plate made of functionally graded material. Based on classical theory of linear thermo-elasticity, Asemi et al. [22] used Rayleighe Ritz energy method and Crank-Nicolson algorithm to consider transient thermo-elastic behavior of an axisymmetric thick truncated FGM cone. Based on higher order shear deformation theory and the geometric nonlinear theory, Shao et al. [23] investigated nonlinear dynamic of piezoelectric fiber metal laminated (FML) plate using Galerkin and DQM. Based on Green and Lindsay, Lord and Shulman, and coupled thermoelasticity theories, Zenkour [24] carried out exact three-dimensional analysis of the temperature, displacements and stresses of a rectangular plate subjected to thermal shock. Transient response of FGM annular sector plate with arbitrary circular boundary conditions was presented semi analytically by Liang et al.[25] using state space differential quadrature method and Laplace transform. Based on first order shear deformation plate theory, nonlinear dynamic and vibration analysis of FGM piezoelectric plate resting on Pasternak foundations subjected to electro-mechanical load and in thermal environment was performed by Duc et al. [26]. Thermoelastic analysis of thin plate was carried out analytically by Wang et al. [27] using Lord and Shulman theory. Based on a higher-order layer wise theory, Pandey and Pradyumna[28] studied thermally induced vibrations of FGM sandwich plates and shell panels under thermal shock by using finite element formulation. Based on first order shear deformation plate theory, Jafarnezhad and Eslami [29] presented response of an FGM annular plate under lateral thermal shock using Laplace transformation and Galerkin finite element method. Alibeigloo [30] employed generalized coupled thermoelasticity and Fourier series state space technique to study time dependent response of sandwich plate with FGM core under thermal shock. From the above mentioned reviewing the literature, it is evident that 3-D coupled thermoelasticity analysis of simply supported FGM cylindrical panel embedded in piezoelectric layers and subjected to induced voltage and thermal shock has not yet been reported. Applying state space Fourier series approach as well as Laplace transform to the constitutive relations, equation of motion and generalized coupled thermoelasticity heat conduction equation based on the Lord–Shulman theory leads to the first order differential equations in Laplace domain which can be solved analytically . Then, inverse Laplace transformation

is employed to convert the obtained solution in to time domain.

## 2. Formulation and analysis

Functionally graded cylindrical panel bonded to piezoelectric layers with simply supported boundary conditions and geometrical dimension in cylindrical coordinate system according to Fig. 1 is considered. The edges of piezoelectric layers are electrically grounded and panel with initially at the ambient temperature, $T_0$ and applied voltage is suddenly subjected to thermal shock at the outer surface whereas the inner surface as well as four ends has zero temperature difference.

### 2.1 FGM layer

It is suppose that material property of FGM layer varies along the radial direction according to the simple power law with the following relation

$$E = E_m\left(\frac{r}{r_i+h_p}\right)^{m_1},\ \alpha = \alpha_m\left(\frac{r}{r_i+h_p}\right)^{m_2},$$

$$k = k_m\left(\frac{r}{r_i+h_p}\right)^{m_3},\ \rho = \rho_m\left(\frac{r}{r_i+h_p}\right)^{m_4} \tag{1}$$

Where $m_1 = \dfrac{\ln\frac{E_c}{E_m}}{\ln\frac{r_o}{r_i+h_p}}$, $m_2 = \dfrac{\ln\frac{\alpha_c}{\alpha_m}}{\ln\frac{r_o}{r_i+h_p}}$,

$m_3 = \dfrac{\ln\frac{k_c}{k_m}}{\ln\frac{r_o}{r_i+h_p}}$, $m_4 = \dfrac{\ln\frac{\rho_c}{\rho_m}}{\ln\frac{r_o}{r_i+h_p}}$

Governing differential equations of motion in cylindrical coordinate system for FGM layer are

$$\sigma_{r,r} + \tau_{zr,z} + \frac{1}{r}\tau_{r\theta,\theta} + \frac{1}{r}\left(\sigma_r - \sigma_\theta\right) = \rho\frac{\partial^2 u_r}{\partial t^2}$$

$$\tau_{r\theta,r} + \frac{1}{r}\sigma_{\theta,\theta} + \tau_{\theta z,z} + \frac{2}{r}\tau_{r\theta} = \rho\frac{\partial^2 u_\theta}{\partial t^2}$$

$$\tau_{zr,r} + \frac{1}{r}\tau_{z\theta,\theta} + \sigma_{z,z} + \frac{1}{r}\tau_{zr} = \rho\frac{\partial^2 u_z}{\partial t^2} \tag{2}$$

Stress-strain relations are

$$\sigma_r = \frac{E}{(1+\nu)(1-2\nu)}\left[(1-\nu)\varepsilon_r + \nu\varepsilon_\theta + \nu\varepsilon_z\right] - \frac{\alpha E}{1-2\nu}T$$

$$\sigma_\theta = \frac{E}{(1+\nu)(1-2\nu)}\left[\nu\varepsilon_r + (1-\nu)\varepsilon_\theta + \nu\varepsilon_z\right] - \frac{\alpha E}{1-2\nu}T$$

$$\sigma_z = \frac{E}{(1+\nu)(1-2\nu)}\left[\nu\varepsilon_r + \nu\varepsilon_\theta + (1-\nu)\varepsilon_z\right] - \frac{\alpha E}{1-2\nu}T$$

$$\tau_{zr} = \frac{E}{2(1+\nu)}\gamma_{zr} \qquad \tau_{r\theta} = \frac{E}{2(1+\nu)}\gamma_{r\theta}$$

$$\tau_{z\theta} = \frac{E}{2(1+\nu)}\gamma_{z\theta} \tag{3}$$

Strain-displacement relations in linear elasticity are

$$\varepsilon_r = u_{r,r} \qquad \varepsilon_\theta = \frac{1}{r}\left(u_r + u_{\theta,\theta}\right) \qquad \varepsilon_z = u_z$$

$$\gamma_{zr} = u_{z,r} + u_{r,z}$$

$$\gamma_{r\theta} = \frac{1}{r}\left(u_{r,\theta} - u_\theta\right) + u_{\theta,r} \qquad \gamma_{z\theta} = u_{\theta,z} + \frac{1}{r}u_{z,\theta} \tag{4}$$

Equilibrium equation of energy as a function of space and time in cylindrical coordinates are

$$\frac{\partial q_r}{\partial r} + \frac{\partial q_\theta}{r\partial\theta} + \frac{\partial q_z}{\partial z} = R - T_0\frac{\partial S}{\partial t} \tag{5}$$

Where $R$ is internal heat generation and $S$ is entropy with the following relation

$$S = \frac{\rho c}{T_0}\left(T - T_0\right) + \beta\left(\varepsilon_r + \varepsilon_\theta + \varepsilon_z\right) \tag{6}$$

Where $\beta = \dfrac{E\alpha}{1-2\nu}$

Three-dimensional heat conduction equations, without internal heat generation, are

$$q_r+\tau_0\frac{\partial q_r}{\partial t}=-k\frac{\partial T}{\partial r} \qquad q_\theta+\tau_0\frac{\partial q_\theta}{\partial t}=-k\frac{\partial T}{r\partial\theta}$$

$$q_z+\tau_0\frac{\partial q_z}{\partial t}=-k\frac{\partial T}{\partial z} \qquad (7)$$

Following equation is derived from Eqs.(4)-(7)

$$\frac{\partial q}{\partial r}=\left[-k\left(\frac{\partial^2}{r^2\partial\theta^2}+\frac{\partial^2}{\partial z^2}\right)+\rho c\left(\frac{\partial}{\partial t}+\tau_0\frac{\partial^2}{\partial t^2}\right)\right]T+ T_0\beta\left(\frac{\partial}{\partial t}+\tau_0\frac{\partial^2}{\partial t^2}\right)\left(\frac{\partial u_r}{\partial r}+\frac{\partial u_z}{\partial z}+\frac{1}{r}\left(u_r+\frac{\partial u_\theta}{\partial\theta}\right)\right) \qquad (8)$$

Where $q=k\frac{\partial T}{\partial r}$

Relations for electric and thermal edges and surfaces boundary conditions for simply supported cylindrical panel are

$$\sigma_z=0,\ u_r=u_\theta=0,\quad \psi=0 \quad \text{at} \quad z=0,\ L \qquad (9a)$$

$$\sigma_\theta=0,\ u_r=u_z=0,\quad \psi=0 \quad \text{at} \quad \theta=0,\ \theta_m \qquad (9b)$$

$$\sigma_r=\tau_{zr}=\tau_{r\theta}=0 \quad T=T_2\sin(p_n z)\sin(p_m\theta)H(t)$$

$$\psi=V \quad \text{at} \quad r=r_o \qquad (9\text{-}c)$$

$$\sigma_r=\tau_{zr}=\tau_{r\theta}=0 \quad D_r=0 \quad \text{at} \quad r=r_i \qquad (9\text{-}d)$$

Where $P_n=n\pi/L$ , $P_m=m\pi/\theta_m$ and $H(t)$ is Heaviside unit step function.

Following Fourier series expansion for stress and displacement components satisfy simply supported boundary condition relations, Eqs.(9a)-(9b)

$$u_r=\sum_{n=1}^{\infty}\sum_{m=1}^{\infty}U_r\sin(p_n z)\sin(p_m\theta)$$

$$u_\theta=\sum_{n=1}^{\infty}\sum_{m=1}^{\infty}U_\theta\sin(p_n z)\cos(p_m\theta)$$

$$u_z=\sum_{n=1}^{\infty}\sum_{m=1}^{\infty}U_r\cos(p_n z)\sin(p_m\theta)$$

$$\sigma_r=\sum_{n=1}^{\infty}\sum_{m=1}^{\infty}\sigma'_r\sin(p_n z)\sin(p_m\theta)\left(\frac{r}{r_i+h_p}\right)^{m_1}$$

$$\sigma_\theta=\sum_{n=1}^{\infty}\sum_{m=1}^{\infty}\sigma'_\theta\sin(p_n z)\sin(p_m\theta)\left(\frac{r}{r_i+h_p}\right)^{m_1}$$

$$\sigma_z=\sum_{n=1}^{\infty}\sum_{m=1}^{\infty}\sigma'_z\sin(p_n z)\sin(p_m\theta)\left(\frac{r}{r_i+h_p}\right)^{m_1}$$

$$\tau_{rz}=\sum_{n=1}^{\infty}\sum_{m=1}^{\infty}\sigma'_r\cos(p_n z)\sin(p_m\theta)\left(\frac{r}{r_i+h_p}\right)^{m_1}$$

$$\tau_{r\theta}=\sum_{n=1}^{\infty}\sum_{m=1}^{\infty}\tau'_{r\theta}\sin(p_n z)\cos(p_m\theta)\left(\frac{r}{r_i+h_p}\right)^{m_1}$$

$$\tau_{z\theta}=\sum_{n=1}^{\infty}\sum_{m=1}^{\infty}\tau'_{z\theta}\cos(p_n z)\cos(p_m\theta)\left(\frac{r}{r_i+h_p}\right)^{m_1}$$

$$T=\sum_{n=1}^{\infty}\sum_{m=1}^{\infty}T'\sin(p_n z)\sin(p_m\theta) \qquad (10)$$

Where $U_i,\sigma'_i\ (i=r,\theta,z)$, $\tau'_{rz}$, $\tau'_{r\theta}$ and $\tau'_{z\theta}$ are function of r and time to be determined.

For simplicity, following non dimensional quantities are introduced

$$\left(\bar\sigma_r\ \ \bar\sigma_\theta\ \ \bar\sigma_z\ \ \bar\tau_{r\theta}\ \ \bar\tau_{rz}\ \ \bar\tau_{z\theta}\right)=\left(\sigma'_r\ \ \sigma'_\theta\ \ \sigma'_z\ \ \tau'_{r\theta}\ \ \tau'_{rz}\ \ \tau'_{z\theta}\right)\frac{1}{Y_0\alpha_0T_0}$$

, $\bar T=\frac{T}{T_0}$

$$\left(\bar U_r\ \ \bar U_\theta\ \ \bar U_z\right)=\left(U_r\ \ U_\theta\ \ U_z\right)\frac{1}{h\alpha_0T_0}, \qquad \bar\rho=\frac{\rho}{\rho_0},$$

$\bar p_n=Lp_n$, $\bar p_m=p_m\theta_m$ , $\bar E=\frac{E}{Y_0}$,

$$\bar\alpha_i=\frac{\alpha_i}{\alpha_0} \quad , \qquad \bar c=\frac{c}{c_0}, \qquad \bar\beta_i=\frac{\beta_i}{Y_0\alpha_0}\ (i=r,\theta,z),$$

$$\bar t=\frac{K_0}{R^2\rho_0c_0}t,\ \bar\tau_0=\frac{K_0}{R^2\rho_0c_0}\tau_0,\ \bar q=\frac{R}{K_0T_0}q$$

$$\left(\begin{array}{ccc}\bar{D}_r & \bar{D}_\theta & \bar{D}_z\end{array}\right)=\left(\begin{array}{ccc}D'_r & D'_\theta & D'_z\end{array}\right)\frac{1}{Y_0\alpha_0T_0|d_1|},$$

$$\bar{\psi}=\frac{|d_1|\psi'}{\alpha_0T_0h},\quad \bar{k}_i=\frac{k_i}{k_0}\quad (i=r,\ \theta,\ z)$$

$$\left(\begin{array}{ccc}\bar{E}_r & \bar{E}_\theta & \bar{E}_z\end{array}\right)=\left(\begin{array}{ccc}\frac{h}{R_m}E_r & \frac{h}{R_m}E_\theta & \frac{h}{L}E_z\end{array}\right)\frac{|d_1|}{\alpha_0T_0},$$

$$\left(\begin{array}{ccc}\bar{\eta}_1 & \bar{\eta}_2 & \bar{\eta}_3\end{array}\right)=\left(\begin{array}{ccc}\eta_1 & \eta_2 & \eta_3\end{array}\right)\frac{1}{Y_0|d_1|^2}$$

$$\left(\begin{array}{ccccc}\bar{e}_1 & \bar{e}_2 & \bar{e}_3 & \bar{e}_4 & \bar{e}_5\end{array}\right)=\left(\begin{array}{ccccc}e_1 & e_2 & e_3 & e_4 & e_5\end{array}\right)\frac{1}{Y_0|d_1|}$$

$$,\ \bar{C}_{ij}=\frac{C_{ij}}{Y_0},\quad \bar{p}_3=\frac{p_3}{Y_0\alpha_0|d_1|},\ \left(\begin{array}{cc}\bar{h}_p & \bar{h}_f\end{array}\right)=\left(\begin{array}{cc}h_p & h_f\end{array}\right)\frac{1}{h}$$

$$\left(\begin{array}{cc}\bar{r} & \bar{z}\end{array}\right)=\left(\begin{array}{cc}\frac{r}{R_m} & \frac{z}{L}\end{array}\right) \tag{11}$$

Using Eqs.(1)-(4), (8), (10)-(11) leads to the following dimensionless state space equations

$$\frac{d\delta_f}{d\bar{z}}=G_f\delta_f \tag{12}$$

Where $\delta_f=\left\{\begin{array}{cccccccc}\bar{\sigma}_r & \bar{U}_r & \bar{U}_\theta & \bar{U}_z & \bar{\tau}_{r\theta} & \bar{\tau}_{rz} & \bar{T} & \bar{q}\end{array}\right\}^T$ is column matrix of state variables and $G_f$ is square coefficient matrix (see appendix)

Accompanied with the state equation, the induced variables are obtained as

$$\left\{\begin{array}{c}\bar{\sigma}_z\\ \bar{\sigma}_\theta\\ \bar{\tau}_{z\theta}\end{array}\right\}=\left[F_f\right]\left[\begin{array}{ccccc}\bar{\sigma}_r & \bar{U}_z & \bar{U}_\theta & \bar{U}_r & \bar{T}\end{array}\right]^T \tag{13}$$

Where $\left[F\right]$ is the matrix of constant coefficients (see appendix)

## 2.2 Piezoelectric layers

Thermo-piezo-elastic constitutive equations of an orthotropic piezoelectric layer in Cartesian coordinate system (x, y, z) are

$$\sigma=C\varepsilon-e^TE-\beta T \tag{14-a}$$

$$D=e\varepsilon+\eta E+p_3T \tag{14-b}$$

Where $\sigma=\left[\begin{array}{cccccc}\sigma_z & \sigma_\theta & \sigma & \tau_r & \tau_\theta & \tau_r\end{array}\right]^T$

$$\varepsilon=\left[\begin{array}{cccccc}\varepsilon_z & \varepsilon_\theta & \varepsilon_r & \gamma_{r\theta} & \gamma_{zr} & \gamma_{z\theta}\end{array}\right]^T$$

$$E=\left[\begin{array}{ccc}E_z & E_\theta & E_r\end{array}\right]^T \qquad D=\left[\begin{array}{ccc}D_z & D_\theta & D_r\end{array}\right]^T$$

$$\beta=\left[\begin{array}{cccccc}\beta_r & \beta_\theta & \beta_z & 0 & 0 & 0\end{array}\right]^T,\ P=\left[\begin{array}{ccc}0 & 0 & p_3\end{array}\right]^T$$

$$C=\begin{bmatrix} C_{11} & C_{12} & C_{13} & 0 & 0 & 0 \\ C_{12} & C_{22} & C_{23} & 0 & 0 & 0 \\ C_{13} & C_{23} & C_{33} & 0 & 0 & 0 \\ 0 & 0 & 0 & C_{44} & 0 & 0 \\ 0 & 0 & 0 & 0 & C_{55} & 0 \\ 0 & 0 & 0 & 0 & 0 & C_{66} \end{bmatrix}$$

$$e=\begin{bmatrix} 0 & 0 & 0 & 0 & e_5 & 0 \\ 0 & 0 & 0 & e_4 & 0 & 0 \\ e_1 & e_2 & e_3 & 0 & 0 & 0 \end{bmatrix}, \eta=\begin{bmatrix} \eta_1 & 0 & 0 \\ 0 & \eta_2 & 0 \\ 0 & 0 & \eta_3 \end{bmatrix} \quad (15)$$

Differential equations of motion and strain-displacement relations for piezoelectric layers are the same as Eqs. (2) and (4) respectively. Electrostatics for elastic deformations of the panel is

$$D_{r,r}+\frac{D_r}{r}+\frac{D_{\theta,\theta}}{r}+D_{z,z}=0 \quad (16)$$

Electric field-electric potential relation in three dimensions are

$$E_r=-\psi_{,r} \qquad E_\theta=-\frac{1}{r}\psi_{,\theta} \qquad E_r=-\psi_{,z} \quad (17)$$

It is noted that electric potential, $\psi$ , at the bottom surface of actuator and top surface of sensor is zero. Following Fourier series expansion for the electric potential and electric displacement satisfy the simply supported boundary conditions.

$$\psi=\sum_{n=1}^{\infty}\sum_{m=1}^{\infty}\bar{\psi}\sin\left(\beta_m\theta\right)\mathrm{in}\left(p_n z\right)$$

$$D_r=\sum_{n=1}^{\infty}\sum_{m=1}^{\infty}D'_r\sin\left(p_n z\right)\sin\left(p_m\theta\right) \quad (18)$$

Equations of energy balance and entropy for piezoelectric layers are the same as Eqs.(5) and (6), respectively. In the absence of internal heat generation, three dimensional heat conduction equations are

$$q_r+\tau_0\frac{\partial q_r}{\partial t}=-k_r\frac{\partial T}{\partial r} \qquad q_\theta+\tau_0\frac{\partial q_\theta}{\partial t}=-k_\theta\frac{\partial T}{r\partial\theta}$$

$$q_z+\tau_0\frac{\partial q_z}{\partial t}=-k_z\frac{\partial T}{\partial z} \quad (19)$$

By using Eqs. (5)-(6) and (19), following equation can be obtained

$$\frac{\partial q}{\partial r}=\left[-k_\theta\frac{\partial^2}{r^2\partial\theta^2}-k_z\frac{\partial^2}{\partial z^2}+\rho c\left(\frac{\partial}{\partial t}+\tau_0\frac{\partial^2}{\partial t^2}\right)\right]T+ T_0\beta\left(\frac{\partial}{\partial t}+\tau_0\frac{\partial^2}{\partial t^2}\right)\left(\frac{\partial u_r}{\partial r}+\frac{\partial u_z}{\partial z}+\frac{1}{r}\left(u_r+\frac{\partial u_\theta}{\partial\theta}\right)\right) \quad (20)$$

Where $q=k_r\frac{\partial T}{\partial r}$

Using Eqs.(2),(4), (10)-(11), (14a,b), (16)-(20) leads to the following dimensionless state space differential equations

$$\frac{d}{d\bar{r}}\delta_p=G_p\delta_p \quad (21)$$

Here

$$\delta_p=\left\{\bar{\sigma}_r \quad \bar{U}_r \quad \bar{U}_\theta \quad \bar{U}_z \quad \bar{\tau}_{zr} \quad \bar{\tau}_{r\theta} \quad \bar{T} \quad \bar{q} \quad \bar{D}_r \quad \bar{\psi}\right\}^T$$

and $G_p$ is constant coefficients square matrix (Appendix ).

Using Eqs. (10), (11) and (14a,b), in-plane stresses in term of state variables can be obtained as the follow

$$\begin{Bmatrix} \bar{\sigma}_z \\ \bar{\sigma}_\theta \\ \bar{\tau}_{z\theta} \end{Bmatrix}=\left[F_p\right]\begin{bmatrix} \bar{\sigma}_r & \bar{U}_z & \bar{U}_\theta & \bar{U}_r & \bar{T} & \bar{D}_r \end{bmatrix}^T \quad (22)$$

Where $\left[F_a\right]$ is coefficient matrix (Appendix).

## 3. Solution procedure

Before solving governing equations it is convenient to transform Eqs. (12) and (21) into Laplace domain as follows

$$\frac{d\hat{\delta}_f}{d\bar{r}} = \hat{G}_f \hat{\delta}_f \tag{23}$$

Here $\hat{\delta}_f = \left\{ \hat{\sigma}_r \quad \hat{U}_z \quad \hat{U}_\theta \quad \hat{U}_r \quad \hat{\tau}_{zr} \quad \hat{\tau}_{r\theta} \quad \hat{T} \quad \hat{q} \right\}^T$ are the state variables in Laplace domain, and $\hat{G}_f$ is Laplace transform of $G_f$ (Appendix).

Since $\hat{G}_f$ is not constant so to solve Eq.(23) analytically, it should be changed to constant matrix. In this paper, FGM layer is divided into N fictitious coaxial thin layers. The coefficient matrix $\hat{G}_f$ at the mid radius of the k-th layer can be assumed to be constant matrix $\hat{G}_{fk}$. Hence solution to Eq. (12) for k-th layer is

$$\delta_{fk}(\bar{r}) = \delta_{0k} e^{\hat{G}_{fk}(\bar{r}-\bar{r}_{k-1})} \qquad \bar{r}_{k-1} \le \bar{r} \le \bar{r}_k \tag{24}$$

Where $\bar{r}_{k-1} = 1 - \frac{\bar{h}_f}{2} + \frac{(k-1)\bar{h}_f}{N}$, $\bar{r}_k = 1 - \frac{\bar{h}_f}{2} + \frac{k\bar{h}_f}{N}$, $\delta_{0k} = \delta_{fk}\big|_{\bar{r}=\bar{r}_{k-1}}$

Eq. (24) at $\bar{r} = \bar{r}_k$ is

$$\delta_{fk}(\bar{r}_k) = M_{fk}\delta_{0k} \tag{25}$$

Where $M_{fk} = \exp\left(\hat{G}_{fk}\frac{\bar{h}_f}{N}\right)$

By using continuity of displacements and equilibrium of traction at each fictitious interface, relation between state variables at inner and outer surfaces of the FGM layer can be written as

$$\delta_f\left(1 + \frac{\bar{h}_f}{2}\right) = M_f \delta_f\left(1 - \frac{\bar{h}_f}{2}\right) \tag{26}$$

Here $M_f = \Pi_{k=N}^{1} \exp\left(\frac{\bar{h}_f \hat{G}_{fk}}{N}\right)$, and $\delta_{fi}$, $\delta_{fo}$ are the state variables at the inner and outer surface of FGM layer, respectively.

Employing the same procedure to Eq. (21), as was used for the FGM layer, leads to the following solution for the j-th fictitious layer of sensor and actuator layers, respectively

$$\delta_{sj}(\bar{r}) = \delta_{0j} e^{\hat{G}_{sj}(\bar{r}-\bar{r}_{j-1})} \qquad \bar{r}_{j-1} \le \bar{r} \le \bar{r}_j \tag{27a}$$

Here $\bar{r}_{j-1} = \bar{r}_i + \frac{(j-1)\bar{h}_p}{M}$, $\bar{r}_j = \bar{r}_i + \frac{j\bar{h}_p}{M}$, $\delta_{0j} = \delta_{sj}\big|_{\bar{r}=\bar{r}_{k-1}}$, M and s denotes the number of fictitious layers and sensor layer, respectively

$$\delta_{aj}(\bar{r}) = \delta_{0j} e^{\hat{G}_{aj}(\bar{r}-\bar{r}_{j-1})} \qquad \bar{r}_{j-1} \le \bar{r} \le \bar{r}_j \tag{27b}$$

Where $\bar{r}_{j-1} = \bar{r}_o - \frac{(M-j-1)\bar{h}_p}{M}$, $\bar{r}_j = \bar{r}_o - \frac{(M-j)\bar{h}_p}{M}$, $\delta_{0j} = \delta_{aj}\big|_{\bar{r}=\bar{r}_{k-1}}$ and a refers to actuator.

Using the same procedure in Eqs. (27a) and (27b), which has been used in deriving Eq.(26) , results in the following relation between state variables at bottom and top surfaces of the sensor and actuator layers, respectively

$$\delta_s(\bar{r}_i + \bar{h}_p) = M_s \delta_s(0) \tag{28a}$$

$$\delta_a(\bar{r}_o) = M_a \delta_a(\bar{r}_o - \bar{h}_p) \tag{28b}$$

Where $M_s = \Pi_{j=M}^{1} \exp\left(\frac{\bar{h}_p \hat{G}_{sj}}{M}\right)$, $M_a = \Pi_{j=M}^{1} \exp\left(\frac{\bar{h}_p \hat{G}_{aj}}{M}\right)$ and $\delta_s(0)$, $\delta_a(\bar{r}_o - \bar{h}_p)$, $\delta_s(\bar{r}_i + \bar{h}_p)$, $\delta_a(\bar{r}_o)$ are state vectors at the inner and outer surface of sensor and actuator layers, respectively. Electric displacement at the bottom surface of actuator layer is derived from Eq. (28b) as follow

$$\bar{D}_z(1 - \bar{h}_p) = \frac{1}{m^a_{109}}\left[\bar{\psi}(1) - \left[m^a_{10j}\right]\delta^m_p(1 - \bar{h}_p)\right] \quad j = 1,....,8 \tag{29}$$

Here $m^a_{109}$ is the 10th row of matrix $M_a$ and $\delta^m_p\left(1-\bar{h}_p\right)$ are mechanical part of state variables of actuator at lower surface.

Substitution of Eq. (29) into the Eq. (28b) and setting $\psi\left(1-\bar{h}_p\right)=0$ results in the following relation

$$\delta^m_p(1)=T_a\delta^m_p\left(1-\bar{h}_p\right)+B \tag{30}$$

Here $T_a=\left(\left[m^a_{ij}\right]-\left\{m^a_{i9}\right\}\left[m^a_{10j}\right]\right)\frac{1}{m^a_{109}}$ ,

$B=\left\{m^a_{i9}\right\}\frac{\psi(h)}{m^a_{109}}$ and $\left\{m^a_{i9}\right\}$ is the 9th column of matrix $M_a$ and

$$\delta^m=\left\{\bar{\sigma}_r \quad \bar{U}_r \quad \bar{U}_\theta \quad \bar{U}_z \quad \bar{\tau}_{zr} \quad \bar{\tau}_{r\theta} \quad \bar{T} \quad \bar{q}\right\}^T$$

$i=j=1,2...,8$

Electric potential, $\psi$ , at the inner surface of sensor is computed from Eq. (28-a) as follow

$$\psi(0)=\frac{-1}{m^s_{1010}}\left[m^s_{10j}\right]\delta^s_p(0) \qquad j=1,\ldots,10 \tag{31}$$

Here $m^s_{10j}$ is the 10th row of matrix $M_s$ and $\delta^s_p(0)$ are mechanical part of state variables at the lower surface of sensor.

Substitution of Eq. (31) into the Eq. (28-a) and setting $D_z(0)=0$ , leads to the following relation

$$\delta^m_p\left(\bar{h}_p\right)=T_s\delta^m_p(0) \tag{32}$$

Here $T_s=\left(\left[m^s_{ij}\right]-\left\{m^s_{i10}\right\}\left[m^s_{10k}\right]\right)\frac{1}{m^s_{1010}}$

$i=j=1,2,....,8$

Applying continuity of state variables at the piezoelectric/FGM interfaces to Eqs. (26), (30) and (32) leads to the following relations between the state variables at the outer and the inner surfaces of the hybrid FGM cylindrical shell

$$\delta\left(\bar{r}_o\right)=K\delta(0)+B \tag{33}$$

Here $K=T_a\times I_f\times M_f\times T_s$ and $I_f$ is square matrix (Appendix).

Applying electro-thermo-mechanical surface boundary conditions, Eqs. (9c)-(9d), to Eq. (33) leads to the following matrix equation in term of displacement components and temperature at the bottom surface of the sensor layer

$$\begin{bmatrix} K_{12} & K_{13} & K_{14} & K_{17} \\ K_{52} & K_{53} & K_{54} & K_{57} \\ K_{62} & K_{63} & K_{64} & K_{67} \\ K_{72} & K_{73} & K_{74} & K_{77} \end{bmatrix}\begin{Bmatrix} \bar{U}_z \\ \bar{U}_\theta \\ \bar{U}_r \\ \bar{q} \end{Bmatrix}_{\bar{r}=\bar{r}_i} = -\begin{Bmatrix} B_1 \\ B_5 \\ B_6 \\ B_7 \end{Bmatrix}+\begin{Bmatrix} 0 \\ 0 \\ 0 \\ \bar{T}_2 \end{Bmatrix} \tag{34}$$

Substitution of obtained displacement components from Eq.(34) into Eqs.(24), (27a) and (27b) results in displacement, transverse stress field and temperature gradient along the radial direction. Moreover, in-plane normal and shear stresses are computed by using the obtained state variables in Eqs. (13) and (22). Finally, obtained results are converted to the time domain via applying inverse Laplace transform.

## 4. Results and discussion

Consider a simply supported FGM cylindrical panel with the following material properties and integrated with piezoelectric sensor and actuator layers with the material properties according to Table 1;

Zirconia: $E_c = 227.24$ GPa , $\alpha_c = 10\times10^{-4}$ / K ,

$k_c = 2.09$ W / mK ,

$\rho_c = 5331$ kg / $m^3$

$c_c = 456.7$ J / kgK

Monel : $E_m = 125.83\ \text{GPa}$, $\alpha_m = 9.5\times10^{-4}\ /\ \text{K}$,

$k_c = 7.5\ \text{W/mK}$,

$\rho_c = 4420\ \text{kg/m}^3$

$c_m = 537\ \text{J/kgK}$

$\frac{h_f}{h_p} = 20$, $\frac{L}{R} = 3$, $\frac{R}{h} = 10$, $\bar{T}_2 = \frac{T_2 - T_0}{T_0}$,

$T_0 = 300\ ^{o}\text{K}$

Where $T_0$ is initial temperature .

Since coupled thermoelasticity analysis of FGM cylindrical panel embedded in piezoelectric layers under thermal shock has not yet been reported in literature so it is not possible to assess validity of the present approach directly. Before, uncoupled thermoelasticity behavior of FGM cylindrical panel integrated with piezoelectric layers subjected to temperature gradient has been studied by author [20] using state space Fourier series method. In other word, changing the thermal shock to temperature difference and using uncoupled thermoelasticity formulation in this formulation, the results are equal to the results reported in the above mentioned reference. Moreover, present paper is extension of work presented in Ref. [30]. It should be noted that the present three dimensional coupled thermoelasticity solution, can be used to validate application range of approximate conventional two dimensional formulation in the future works. In what follows, numerical illustration for time history as well as through the thickness distribution of stresses, displacements, temperature and induced voltage are computed and plotted in Figs. 2-6 and tabulated in Table 2. Time history of stresses, displacements and temperature at mid radius of hybrid FGM cylindrical panel with different thermal relaxation time are represented in Figs.2a-2f. From the figures it is observed that increase thermal relaxation time causes to increase all of quantities. This is due to the increasing applied thermal shock loading compared to the static loading. According to the figures, effect of $\bar{\tau}_o$ on stresses is more significant than that on the displacements. Distribution of stresses, displacements, induced voltage and temperature along the radial direction for various peak values of thermal shock are depicted in Figs.3a-3f. According to the figures and as expected, stresses, displacement, voltage and temperature gradient increase by increasing applied temperature difference at top surface. Moreover, continuity of displacements and transverse normal and shear stresses are exactly satisfied. In addition, from Figs. 3a-3c it is concluded that influence of thermal shock on stress distribution for FGM layer is more noticeable. According to Figs.3d-3f, radial and axial displacement as well as temperature at the top surface is more affected than that at the bottom surface. Distribution of temperature along the thickness direction in FGM layer is nonlinear whereas it is linear in piezoelectric layers (Fig.3f). It should be noted that this is due to the variation of thermal conductivity coefficient according to power law along the thickness direction in FGM layer whereas it is constant in piezoelectric layers. Figs.4a-4c represents effect of applied voltage on stress and displacement fields of FGM hybrid cylindrical panel in the absence of thermal shock. According to the figures increase applied voltage causes to increase all of physical quantities. Effect of applied voltage on stresses and displacement at the top surface is noticeable which is due to the applied voltage at the top surface. Moreover, it is observed that increase applied voltage causes to increase nonlinearity of through-thickness distribution of stresses and displacement. Effect of mid radius to thickness ratio on through the thickness distribution of stresses and displacements is depicted in Figs. 5a-5c. Increase mid radius to thickness ratio causes to decrease the stiffness of the panel and consequently stresses decrease whereas deflection increase. Furthermore, it is concluded that by increasing, $S = \frac{R}{h}$, stresses converge to a constant value which

denotes the thin shell behavior. Effect of FGM to piezoelectric thickness ratio on time history of stresses and displacements of hybrid FGM cylindrical panel is demonstrated in Figs.6a-6c. Since piezoelectric layers are measuring instrument so in the absence of applied voltage they should not affect the behavior of FGM layer. For this reason thickness of the sensor and actuator layers compared to the FGM layer thickness should be selected such that to provide this behavior. From the figures it can be concluded that increase $\frac{h_f}{h_p}$ causes to converge stresses and displacement to a constant value. In this paper when $\frac{h_f}{h_p}=100$, influence of piezoelectric layers on the bending behavior of FGM layer in the absence of voltage is negligible. Effect of thermal relaxation time on Non dimensional stresses and displacements at mid radius of FGM hybrid panel with different mid radius to thickness ratio are presented in Table 2. From table it can be observed that regardless of, S by increasing $\tau_o$ stresses, radial and axial displacement increase whereas circumferential displacement decreases. Besides, it is concluded that effect of $\tau_o$ on stress and displacement fields is noticeable in thick FGM panel compared to the thin panel.

## 5. Conclusion

Three dimensional coupled thermo-electro-elastic behavior of simply supported FGM cylindrical panel imbedded in piezoelectric layers and subjected to thermal shock was investigated. Thermo-elastic material properties of FGM layer are supposed to vary according to power law function of radial coordinate. Based on the Lord–Shulman theory, analysis was carried out by using Fourier series state-space approach for space domain and Laplace transform for time domain. From parametric study it was concluded that the material inhomogeneity significantly affect coupled thermoelastic behavior of the hybrid FGM cylindrical panel. Moreover, following additional conclusions are made;

- Effect of $\bar{\tau}_o$ on stresses is more significant than that on the displacements.
- Due to the FGM, distribution of stresses, displacements and temperature along the radial direction vary nonlinearly in host layer whiles they vary linearly for the piezoelectric layers.
- Effect of thermal shock on stresses, displacement and temperature at the top surface is more significant than that at the bottom surface.
- Variation of thermal stress in FGM layer, compared to piezoelectric layers, is more considerable.
- By increasing thermal shock, nonlinearity of distribution of displacement increase.
- Increase mid-radius to thickness ratio stresses converge to a constant value which denotes the thin shell behavior.
- When piezoelectric thickness riches to a specified value its effect on bending behavior of FGM layer a in the absence of voltage is negligible.
- Effect of $\tau_o$ on stress and displacement fields in thick FGM panel is noticeable.

## 6. Figures

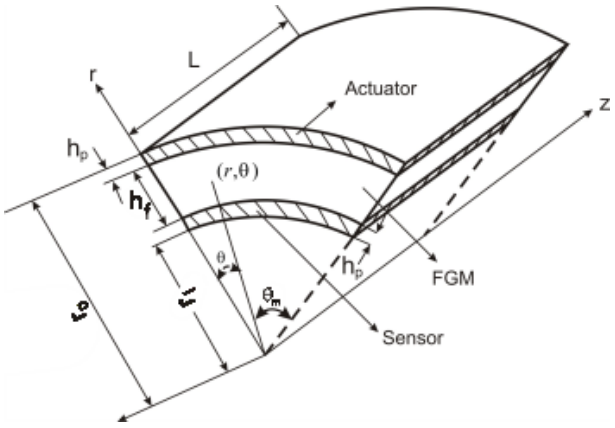


**Fig.1.** Geometry of the hybrid FGM cylindrical panel

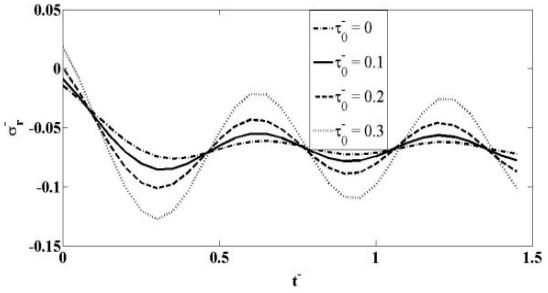


a) Radial normal stress

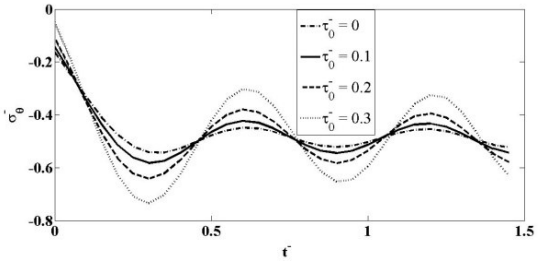


b) Circumferential normal stress

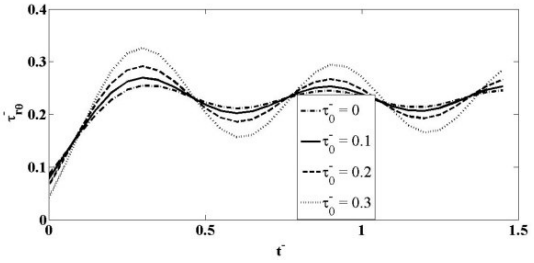


c) Transverse shear stress

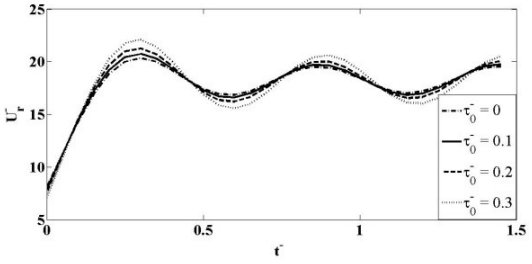


d) Deflection

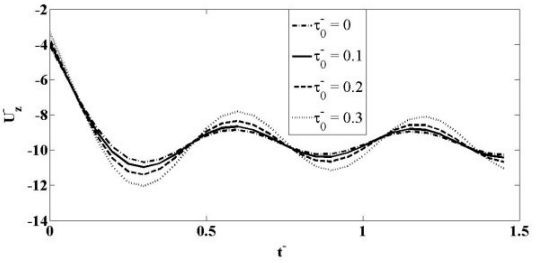


e) Axial displacement

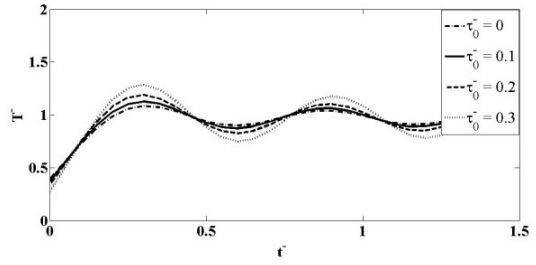


f) Temperature

**Fig. 2.** Time history of stresses, displacements and temperature at the mid-radius of hybrid cylindrical FGM panel with different thermal relaxation constant, $\bar{\tau}_0$ , $\bar{T}_2 = 2$ and $\bar{\psi} = 0$

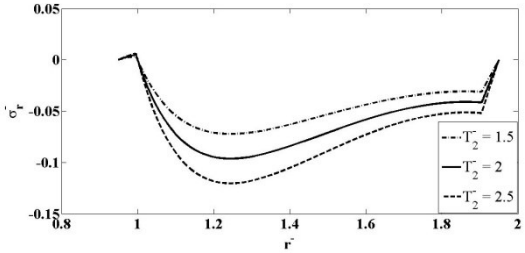


a) Transverse normal stress

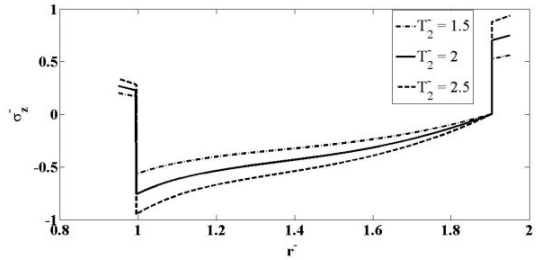


b) Axial normal stress

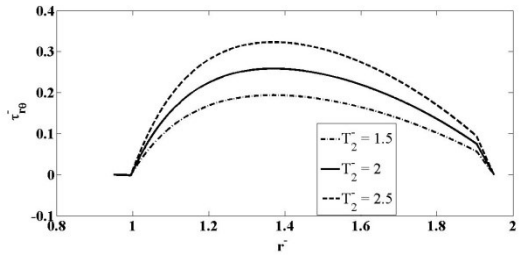


c) Transverse shear stress

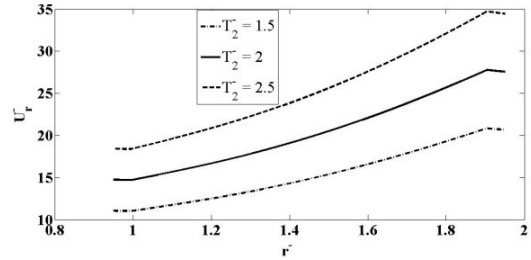


d) Deflection

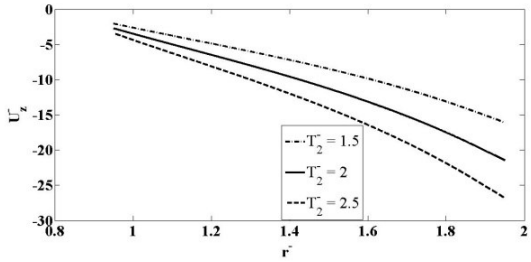


e) Axial displacement

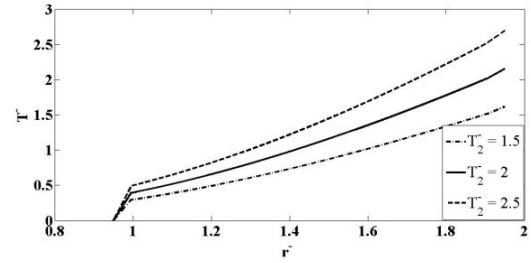


f) Temperature

**Fig. 3.** Through thickness distribution of stresses, temperature and displacements of hybrid FGM cylindrical panel with different thermal shock and $\bar{\tau}_o = 0.1$ , $\bar{T}_2 = 2$ , $\bar{t} = 1.5$ , $\bar{\psi} = 0$ .

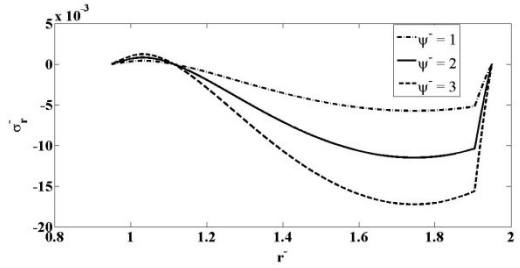


a) Radial normal stress

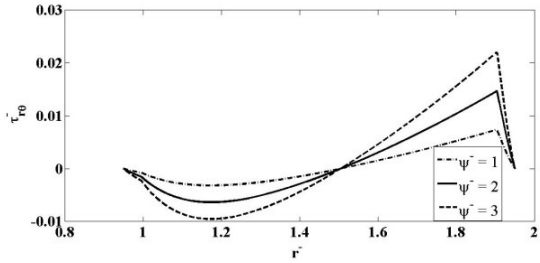


b) Transverse shear stress

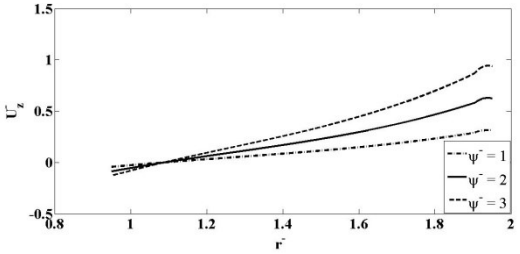


c) Axial displacement

**Fig.4.** Through thickness distribution of stresses and displacements of hybrid FGM cylindrical panel with different applied voltage and $\bar{\tau}_o = 0.1$ , $\bar{t} = 1.5$ , $\bar{T}_2 = 0$ .

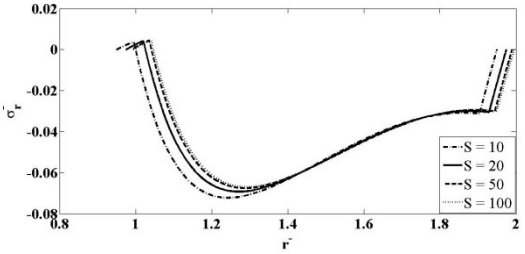


a) Radial normal stress

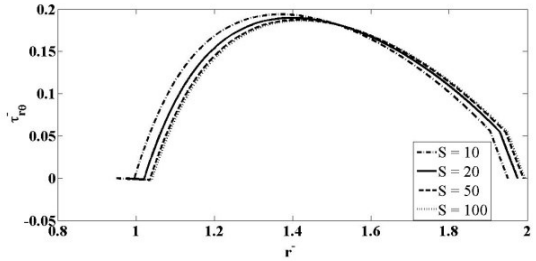


b) Transverse shear stress

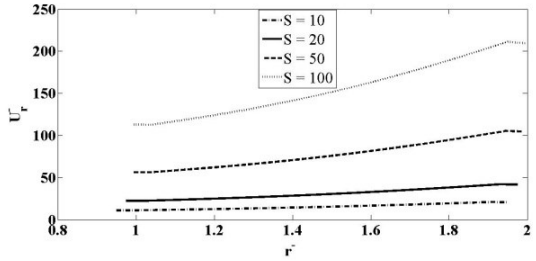


c) Deflection

**Fig. 5.** Effect of mid-radius to thickness ratio on through-thickness distribution of stresses and displacements of hybrid FGM cylindrical panel with $\bar{\tau}_o = 0.1$ , $\bar{t} = 1.5$ , $\bar{T}_2 = 2$ , $\bar{\psi} = 0$ .

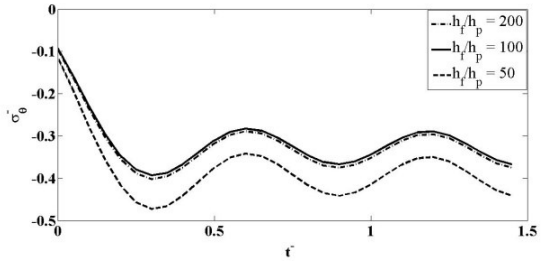


a) Circumferential normal stress

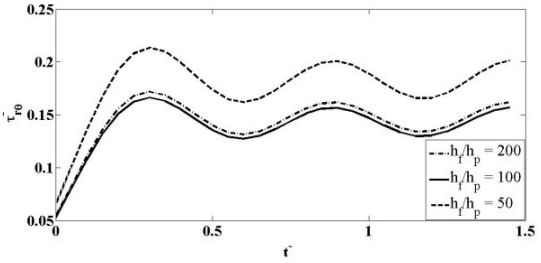


b) Axial normal stress

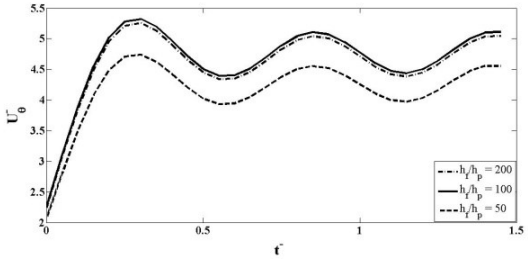


c) Circumferential displacement

**Fig. 6.** Effect of FGM thickness to piezoelectric thickness ratio on time history of stresses and displacements of hybrid FGM cylindrical panel with $\bar{\tau}_o = 0.1$ , $\bar{t} = 1.5$ , $\bar{T}_2 = 2$ , $\bar{\psi} = 0$ .

## 7. Tables

Table 1. Material properties of piezoelectric sensor and actuator.

| Property (GPa) | $C_{11}$ | $C_{12}$ | $C_{13}$ | $C_{22}$ | $C_{23}$ | $C_{33}$ | $C_{44}$ | $C_{55}$ | $C_{66}$ | |
|---|---|---|---|---|---|---|---|---|---|---|
| Sensor ( PZT-4) | 139 | 78 | 74 | 139 | 74 | 115 | 25.6 | 25.6 | 30.5 | |
| Actuator $(Ba_2NaNb_5O_{15})$ | 239 | 104 | 5 | 247 | 52 | 135 | 65 | 66 | 76 | |
| Property * | $e_1$ | $e_2$ | $e_3$ | $e_4$ | $e_5$ | $_1\mu$ | $\mu_2$ | $\mu_3$ | $d_1$ | $p_3$ |
| Sensor ( PZT-4) | -5.2 | -5.2 | 15.1 | 12.7 | 12.7 | 6.5e-9 | 6.5e-9 | 5.6e-9 | -3.92e-12 | 5.4 e-5 |
| Actuator $(Ba_2NaNb_5O_{15})$ | 0.4 | -0.3 | 4.3 | 3.4 | 2.8 | 1.96e-9 | 2.01e-9 | 0.28e-9 | -3.92e-12 | 5.4e-5 |

* The unit of matrix e is coul/m$^2$, matrix $\mu$ is farads/m, $d_1$ is coul/N and $p_3$ is coul/m$^2$K

Table 2. Effect of thermal relaxation time on stresses and displacements at mid-radius of hybrid cylindrical Panel with different S

| S | $\tau_o$ | $\bar{\sigma}_r$ | $\bar{\sigma}_\theta$ | $\bar{\sigma}_z$ | $\bar{\tau}_{r\theta}$ | $\bar{U}_r$ | $\bar{U}_\theta$ | $\bar{U}_z$ |
|---|---|---|---|---|---|---|---|---|
| 10 | 0.0 | -0.0545 | -0.3918 | -0.2884 | 0.1841 | 14.6627 | 2.9902 | -7.7034 |
| | 0.1 | -0.0584 | -0.4079 | -0.3042 | 0.1898 | 14.8187 | 2.9777 | -7.8217 |
| | 0.2 | -0.0654 | -0.4340 | -0.3301 | 0.1994 | 15.0580 | 2.9503 | -8.0087 |
| | 0.3 | -0.0760 | -0.4722 | -0.3682 | 0.2137 | 15.3993 | 2.9045 | -8.2800 |
| 20 | 0.0 | -0.0520 | 0.3930 | -0.2827 | 0.1805 | 29.6124 | 5.9416 | -15.5355 |
| | 0.1 | -0.0562 | -0.4093 | -0.2985 | 0.1862 | 29.9303 | 5.9171 | -15.7762 |
| | 0.2 | -0.0632 | -0.4356 | -0.3241 | 0.1957 | 30.4187 | 5.8629 | -16.1574 |
| | 0.3 | -0.0736 | -0.4740 | -0.3618 | 0.2098 | 31.1130 | 5.7728 | -16.7082 |
| 50 | 0.0 | -0.0508 | -0.3938 | -0.2795 | 0.1783 | 74.4502 | 14.7896 | -39.0243 |
| | 0.1 | -0.0549 | -0.4102 | -0.2951 | 0.1840 | 75.2538 | 14.7288 | -39.6322 |
| | 0.2 | -0.0619 | -0.4366 | -0.3207 | 0.1935 | 76.4889 | 14.5942 | -40.5954 |
| | 0.3 | -0.0722 | -0.4751 | -0.3581 | 0.2075 | 78.2416 | 14.3711 | -41.9846 |

## Appendix

$G_f =$

$$\begin{bmatrix} g_{11} & g_{12} & g_{13} & g_{14} & \frac{R}{L}\bar{p}_n & \frac{\bar{p}_m}{\bar{r}\theta_m} & g_{17} & 0 \\ 0 & 0 & 0 & -\frac{R}{L}\bar{p}_n & g_{25} & 0 & 0 & 0 \\ 0 & 0 & \frac{1}{\bar{r}} & -\frac{\bar{p}_m}{\bar{r}\theta_m} & 0 & g_{25} & 0 & 0 \\ g_{41} & g_{42} & g_{43} & g_{44} & 0 & 0 & g_{47} & 0 \\ -g_{42} & g_{52} & g_{53} & g_{54} & \frac{-(m_1+1)}{\bar{r}} & 0 & g_{57} & 0 \\ g_{61} & g_{53} & g_{63} & g_{13} & 0 & \frac{-(m_1+2)}{\bar{r}} & g_{67} & 0 \\ 0 & 0 & 0 & 0 & 0 & 0 & 0 & \frac{1}{\bar{k}_i}\left(\frac{\bar{r}}{\bar{R}_i+\bar{h}_p}\right)^{-m_3} \\ g_{81} & g_{82} & g_{83} & g_{84} & 0 & 0 & g_{87} & 0 \end{bmatrix}$$

Where

$$g_{11} = -\frac{1}{\bar{r}}\left(m_1 + \frac{1-2\nu}{1-\nu}\right) \qquad g_{12} = -\frac{h}{L}\frac{\bar{E}_i \nu \bar{p}_n}{\bar{r}\left(1-\nu^2\right)}$$

$$g_{13} = -\frac{h}{R}\frac{\bar{p}_m}{\theta_m}\frac{\bar{E}_i}{\bar{r}^2\left(1-\nu^2\right)}$$

$$g_{14} = \frac{h}{R}\left(\frac{\bar{E}_i}{\bar{r}^2\left(1-\nu^2\right)} + \frac{k_o^2\bar{\rho}_i}{R^2 Y_o \rho_o c_o^2}\times\left(\frac{\bar{r}}{\bar{R}_i+\bar{h}_p}\right)^{(m_4-m_1)}\times\frac{\partial^2}{\partial t^2}\right)$$

$$g_{17} = -\frac{\bar{E}_i\bar{\alpha}_i}{\bar{r}(1-\nu)}\left(\frac{\bar{r}}{\bar{R}_i+\bar{h}_p}\right)^{m_2}$$

$$g_{25} = \frac{2(1+\nu)}{\bar{E}_i}\frac{R}{h} \qquad g_{41} = \frac{R}{h}\frac{(1+\nu)(1-2\nu)}{\bar{E}_i(1-\nu)} \qquad g_{42} = \frac{R}{L}\frac{\nu\bar{p}_n}{1-\nu}$$

$$g_{43} = \frac{\bar{p}_m}{\theta_m}\frac{\nu}{\bar{r}(1-\nu)} \qquad g_{44} = \frac{-\nu}{\bar{r}(1-\nu)}$$

$$g_{52} = \frac{h}{R}\left(\frac{\bar{E}_i}{1+\nu}\left(\left(\frac{R}{L}\right)^2\times\frac{\bar{p}_n^2}{1-\nu}+\frac{1}{2}\left(\frac{\bar{p}_m}{\bar{r}\theta_m}\right)^2\right)+\frac{k_o^2\bar{\rho}_i}{R^2 Y_o\rho_o c_o^2}\times\left(\frac{\bar{r}}{\bar{R}_i+\bar{h}_m}\right)^{(m_4-m_1)}\times\frac{\partial^2}{\partial t^2}\right)$$

$$g_{47} = \frac{R}{h}\frac{\bar{\alpha}_i(1+\nu)}{(1-\nu)}\left(\frac{\bar{r}}{\bar{R}_i+\bar{h}_m}\right)^{m_2} \qquad g_{53} = \frac{h}{L}\frac{\bar{p}_m}{\theta_m}\frac{\bar{p}_n\bar{E}_i}{2\bar{r}(1-\nu)}$$

$$g_{54} = -\frac{h}{L}\frac{\bar{p}_n\bar{E}_i\nu}{\bar{r}\left(1-\nu^2\right)} \qquad g_{57} = \frac{R}{L}\frac{\bar{E}_i\bar{\alpha}_i\bar{p}_n}{1-\nu}\left(\frac{\bar{r}}{\bar{R}_i+\bar{h}_p}\right)^{m_2}$$

$$g_{61} = -\frac{\bar{p}_m}{\theta_m}\frac{\nu}{\bar{r}(1-\nu)}$$

$$g_{67} = \frac{\bar{p}_m}{\theta_m}\frac{\bar{E}_i\bar{\alpha}_i}{\bar{r}(1-\nu)}\left(\frac{\bar{r}}{\bar{R}_i+\bar{h}_m}\right)^{m_2}$$

$$g_{63} = \frac{h}{R}\left(\frac{\bar{E}_i}{1+\nu}\left(\left(\frac{R}{L}\right)^2\times\frac{\bar{p}_n^2}{2}+\frac{1}{1-\nu}\left(\frac{\bar{p}_m}{\bar{r}\theta_m}\right)^2\right)\right.$$

$$\left.+\frac{k_o^2\bar{\rho}_i}{R^2 Y_o\rho_o c_o^2}\times\left(\frac{\bar{r}}{\bar{R}_i+\bar{h}_m}\right)^{(m_4-m_1)}\times\frac{\partial^2}{\partial t^2}\right)$$

$$g_{81} = D\frac{1+\nu}{\bar{E}_i} \qquad g_{8\ \bar{2}} = -\ D\frac{h}{L}- \qquad g_{83} = -D\frac{h}{R}\frac{\bar{p}_m}{\bar{r}\theta_m}$$

$$g_{84} = D\frac{h}{R}\frac{1}{\bar{r}}$$

Where

$$D = \frac{1}{1-\nu}\frac{\alpha_o^2 Y_o T_o \bar{E}_i\bar{\alpha}_i}{\rho_o c_o}\left(\frac{\bar{r}}{\bar{R}_i+\bar{h}_m}\right)^{m_1+m_2}\left(\frac{\partial}{\partial\bar{t}}+\bar{\tau}_0\frac{\partial^2}{\partial\bar{t}^2}\right)$$

$$g_{87} = \bar{k}_i\left(\frac{\bar{r}}{\bar{R}_i+\bar{h}_m}\right)^{m_3}\left[\left(\frac{R}{L}\bar{p}_n\right)^2+\left(\frac{\bar{p}_m}{\bar{r}\theta_m}\right)^2\right]+\left[\bar{c}_i\bar{\rho}_i\left(\frac{\bar{r}}{\bar{R}_i+\bar{h}_m}\right)^{m_4}\right.$$

$$\left.+\frac{1+\nu}{(1+\nu)(1-2\nu)}\frac{\alpha_o^2 Y_o T_o\bar{E}_i\bar{\alpha}_i}{\rho_o c_o}\times\left(\frac{\bar{r}}{\bar{R}_i+\bar{h}_m}\right)^{(m_1+m_2)}\right]\left(\frac{\partial}{\partial\bar{t}}+\bar{\tau}_0\frac{\partial^2}{\partial\bar{t}^2}\right)$$

$$F_f = \begin{bmatrix} \frac{\nu}{1-\nu} & -\frac{h}{L}\frac{\bar{E}_i\bar{p}_n}{1-\nu^2} & -\frac{h}{R}\frac{\bar{p}_m}{\theta_m}\frac{\bar{E}_i\nu}{\bar{r}(1-\nu^2)} & \frac{h}{R}\frac{\bar{E}_i\nu}{\bar{r}(1-\nu^2)} & -\frac{\bar{E}_i\bar{\alpha}_i}{1-\nu}\left(\frac{\bar{r}}{\bar{r}+\bar{h}_p}\right)^{m_2} \\ \frac{\nu}{1-\nu} & -\frac{h}{L}\frac{\bar{E}_i\bar{p}_n\nu}{1-\nu^2} & -\frac{h}{R}\frac{\bar{p}_m}{\theta_m}\frac{\bar{E}_0}{\bar{r}(1-\nu^2)} & \frac{h}{R}\frac{\bar{E}_i}{\bar{r}(1-\nu^2)} & -\frac{\bar{E}_i\bar{\alpha}_i}{1-\nu}\left(\frac{\bar{r}}{\bar{r}+\bar{h}_p}\right)^{m_2} \\ 0 & \frac{h}{2R}\frac{\bar{p}_m}{\theta_m}\frac{\bar{E}_i}{\bar{r}(1+\nu)} & \frac{h}{2L}\frac{\bar{E}_i\bar{p}_n}{\bar{r}(1+\nu)} & 0 & 0 \end{bmatrix}$$

$$G_p=\begin{bmatrix} a_{11} & a_{12} & a_{13} & a_{14} & \frac{R}{L}\bar{p}_n & \frac{\bar{p}_m}{r\theta_m} & a_{17} & 0 & a_{19} & 0 \\ 0 & 0 & 0 & -\frac{R}{L}\bar{p}_n & a_{25} & 0 & 0 & 0 & 0 & a_{210} \\ 0 & 0 & \frac{1}{\bar{r}} & -\frac{\bar{p}_m}{r\theta_m} & 0 & \frac{R}{h\bar{C}_{44}} & 0 & 0 & 0 & a_{310} \\ a_{41} & a_{42} & a_{43} & a_{44} & 0 & 0 & a_{47} & 0 & a_{49} & 0 \\ a_{51} & a_{52} & a_{53} & a_{54} & -\frac{1}{\bar{r}} & 0 & a_{57} & 0 & a_{59} & 0 \\ a_{61} & a_{62} & a_{63} & a_{64} & 0 & -\frac{2}{\bar{r}} & a_{67} & 0 & a_{69} & 0 \\ 0 & 0 & 0 & 0 & 0 & 0 & 0 & \frac{1}{k_r} & 0 & 0 \\ a_{81} & a_{82} & a_{83} & a_{84} & 0 & 0 & a_{87} & 0 & 0 & 0 \\ 0 & 0 & 0 & 0 & a_{95} & a_{96} & 0 & 0 & -1 & a_{910} \\ a_{101} & a_{102} & a_{103} & a_{104} & 0 & 0 & a_{107} & 0 & a_{109} & 0 \end{bmatrix}$$

where;

$$a_{11}=\frac{1}{\bar{r}}\left(-1+\frac{e_2e_3+C_{23}\eta_3}{C_{33}\eta_3+e_3^2}\right)$$

$$a_{12}=\frac{\bar{p}_n}{\bar{r}}\frac{h}{L}\left[-\bar{C}_{12}+\frac{\bar{C}_{23}\left(\bar{C}_{13}\bar{\eta}_3+\bar{e}_1\bar{e}_3\right)+\bar{e}_2\left(\bar{e}_3\bar{C}_{13}-\bar{e}_1\bar{C}_{33}\right)}{\bar{C}_{33}\bar{\eta}_3+\bar{e}_3^2}\right]$$

$$a_{13}=\frac{h}{R}\frac{p_m}{\theta_m}\frac{1}{\bar{r}^2}\left[-\bar{C}_{22}+\frac{\bar{e}_2\left(\bar{e}_2\bar{C}_{33}-\bar{e}_3\bar{C}_{32}\right)-\bar{C}_{23}\left(\bar{e}_2\bar{e}_3+\bar{C}_{33}\bar{\eta}_3\right)}{\bar{C}_{33}\bar{\eta}_3+\bar{e}_3^2}\right]$$

$$a_{14}=\frac{h}{R}\frac{1}{\bar{r}^2}\left[\bar{C}_{22}+\frac{\bar{e}_2\left(-\bar{e}_2\bar{C}_{33}+\bar{e}_3\bar{C}_{32}\right)+\bar{C}_{23}\left(\bar{e}_2\bar{e}_3+\bar{C}_{33}\bar{\eta}_3\right)}{\bar{C}_{33}\bar{\eta}_3+\bar{e}_3^2}\right]$$

$$a_{17}=\frac{1}{\bar{r}}\left[-\bar{\beta}_\theta+\frac{\bar{C}_{23}\left(\bar{\beta}_r\bar{\eta}_3-\bar{e}_3\bar{p}_3\right)+\bar{e}_2\left(\bar{p}_3\bar{C}_{33}+\bar{e}_3\bar{\beta}_r\right)}{\bar{C}_{33}\bar{\eta}_3+\bar{e}_3^2}\right]$$

$$a_{19}=\frac{1}{\bar{r}}\frac{\bar{C}_{23}\bar{e}_3-\bar{e}_2\bar{C}_{33}}{\bar{C}_{33}\bar{\eta}_3+\bar{e}_3^2} \qquad a_{25}=\frac{R}{h\bar{C}_{55}} \quad a_{210}=\frac{-R\bar{P}_n\bar{e}_5}{L\bar{C}_{55}}$$

$$a_{310}=\frac{-\bar{P}_m\bar{e}_4}{\bar{r}\theta_m\bar{C}_{44}} \qquad a_{41}=\frac{R}{h}\frac{\bar{\eta}_3}{\bar{C}_{33}\bar{\eta}_3+\bar{e}_3^2}$$

$$a_{42}=\frac{R}{L}\frac{\bar{p}_n\left(\bar{C}_{13}\bar{\eta}_3+\bar{e}_1\bar{e}_3\right)}{\bar{C}_{33}\bar{\eta}_3+\bar{e}_3^2}$$

$$a_{43}=\frac{\bar{p}_m}{\theta_m}\frac{\left(\bar{C}_{23}\bar{\eta}_3+\bar{e}_2\bar{e}_3\right)}{\bar{r}\left(\bar{C}_{33}\bar{\eta}_3+\bar{e}_3^2\right)} \qquad a_{44}=-\frac{\left(\bar{C}_2\ \bar{\eta}_3+\bar{e}\ \bar{e}_3\right)}{\bar{r}\left(\bar{C}_{33}\bar{\eta}_3+\bar{e}_3^2\right)}$$

$$a_{47}=-\frac{R}{h}\frac{\bar{\beta}_r\bar{\eta}_3-\bar{e}_3\bar{p}_3}{\bar{C}_{33}\bar{\eta}_3+\bar{e}_3^2} \quad a_{49}=\frac{R}{h}\frac{\bar{e}_3}{\bar{C}_{33}\bar{\eta}_3+\bar{e}_3^2}$$

$$a_{52}=\frac{Rh}{L^2}\bar{p}_n^2\left[\bar{C}_{11}+\frac{\bar{e}_1\left(\bar{C}_{33}\bar{e}_1-\bar{e}_3\bar{C}_{13}\right)-\bar{C}_{13}\left(\bar{C}_{13}\bar{\eta}_3+\bar{e}_1\bar{e}_3\right)}{\bar{C}_{33}\bar{\eta}_3+\bar{e}_3^2}\right]$$

$$+\frac{h}{R}\frac{\bar{p}_m^2}{\bar{r}^2\theta_m^2}\bar{C}_{66}+\frac{h}{R}\bar{\rho}\left(\frac{k_0}{Rc_0}\right)^2\frac{1}{\rho_0Y_0}\frac{\partial^2}{\partial\bar{t}^2}$$

$$a_{53}=\frac{h}{L}\frac{\bar{p}_n}{\bar{r}}\frac{\bar{p}_m}{\theta_m}\left[\bar{C}_{12}+\bar{C}_{66}+\frac{\bar{e}_1\left(\bar{C}_{33}\bar{e}_2-\bar{C}_{32}\bar{e}_3\right)-\bar{C}_{13}\left(\bar{C}_{32}\bar{\eta}_3+\bar{e}_2\bar{e}_3\right)}{\bar{C}_{33}\bar{\eta}_3+\bar{e}_3^2}\right]$$

$$a_{51}=-\frac{R}{L}\frac{\bar{p}_n\left(\bar{C}_{13}\bar{\eta}_3+\bar{e}_1\bar{e}_3\right)}{\bar{r}\left(\bar{C}_{33}\bar{\eta}_3+\bar{e}_3^2\right)}$$

$$a_{54}=\frac{h}{L}\frac{\bar{p}_n}{\bar{r}}\left[-\bar{C}_{12}+\frac{\bar{C}_{13}\left(\bar{e}_2\bar{e}_3+\bar{C}_{32}\bar{\eta}_2\right)-\bar{e}_1\left(\bar{C}_{33}\bar{e}_2-\bar{e}_3\bar{C}_{32}\right)}{\bar{C}_{33}\bar{\eta}_3+\bar{e}_3^2}\right]$$

$$a_{57}=\frac{R}{L}\bar{p}_n\left[\bar{\beta}_z-\frac{\bar{C}_{13}\left(\bar{\beta}_r\bar{\eta}_3-\bar{e}_3\bar{p}_3\right)+\bar{e}_1\left(\bar{p}_3\bar{C}_{33}+\bar{e}_3\bar{\beta}_r\right)}{\bar{C}_{33}\bar{\eta}_3+\bar{e}_3^2}\right]$$

$$a_{59}=\frac{R}{L}\frac{\bar{p}_n\left(\bar{e}_1\bar{C}_{33}-\bar{C}_{13}\bar{e}_3\right)}{\left(\bar{C}_{33}\bar{\eta}_3+\bar{e}_3^2\right)}$$

$$a_{61}=-\frac{\bar{p}_m}{\theta_m}\frac{\left(\bar{C}_{23}\bar{\eta}_3+\bar{e}_2\bar{e}_3\right)}{\bar{r}\left(\bar{C}_{33}\bar{\eta}_3+\bar{e}_3^2\right)}$$

$$a_{62}=\frac{h}{L}\frac{\bar{p}_n}{\bar{r}}\frac{\bar{p}_m}{\theta_m}\left[\bar{C}_{12}+\bar{C}_{66}-\frac{\bar{C}_{23}\left(\bar{C}_{13}\bar{\eta}_3+\bar{e}_1\bar{e}_3\right)+\bar{e}_2\left(\bar{e}_3\bar{C}_{13}-\bar{e}_1\bar{C}_{33}\right)}{\bar{C}_{33}\bar{\eta}_3+\bar{e}_3^2}\right]$$

$$a_{102}=\frac{R}{L}\frac{\bar{p}_n\left(\bar{e}_3\bar{C}_{13}-\bar{e}_1\bar{C}_{33}\right)}{\left(\bar{C}_{33}\bar{\eta}_3+\bar{e}_3^2\right)}$$

$$a_{63}=\frac{h}{R}\frac{\bar{p}_m^2}{\bar{r}^2\theta_m^2}\left[\bar{C}_{22}+\frac{\bar{e}_2\left(\bar{e}_2\bar{C}_{33}-\bar{e}_3\bar{C}_{32}\right)-\bar{C}_{23}\left(\bar{C}_{32}\bar{\eta}_3+\bar{e}_2\bar{e}_3\right)}{\bar{C}_{33}\bar{\eta}_3+\bar{e}_3^2}\right]$$

$$a_{103}=-\frac{\bar{p}_m}{\bar{r}\theta_m}\frac{\bar{e}_2\bar{C}_{33}-\bar{e}_3\bar{C}_{32}}{\bar{C}_{33}\bar{\eta}_3+\bar{e}_3^2}\qquad a_{104}=\frac{1}{\bar{r}}\frac{\bar{e}_2\bar{C}_{33}-\bar{e}_3\bar{C}_{32}}{\bar{C}_{33}\bar{\eta}_3+\bar{e}_3^2}$$

$$+\frac{Rh}{L^2}\bar{p}_n^2\bar{C}_{66}+\frac{h}{R}\bar{\rho}\left(\frac{k_0}{Rc_0}\right)^2\frac{1}{\rho_0 Y_0}\frac{\partial^2}{\partial\bar{\tau}^2}$$

$$a_{107}=\frac{R}{h}\frac{\bar{p}_3\bar{C}_{33}+\bar{e}_3\bar{\beta}_r}{\bar{C}_{33}\bar{\eta}_3+\bar{e}_3^2}\qquad a_{109}=-\frac{R}{h}\frac{\bar{C}_{33}}{\bar{C}_{33}\bar{\eta}_3+\bar{e}_3^2}$$

$$a_{64}=\frac{h}{R}\frac{\bar{p}_m}{\bar{r}^2\theta_m}\left[-\bar{C}_{22}+\frac{\bar{C}_{23}\left(\bar{e}_2\bar{e}_3+\bar{C}_{32}\bar{\eta}_2\right)-\bar{e}_2\left(\bar{C}_{33}\bar{e}_2-\bar{e}_3\bar{C}_{32}\right)}{\bar{C}_{33}\bar{\eta}_3+\bar{e}_3^2}\right]$$

$$a_{67}=\frac{R}{L}\frac{\bar{p}_m}{\bar{r}\theta_m}\left[\bar{\beta}_\theta-\frac{\bar{C}_{23}\left(\bar{\beta}_r\bar{\eta}_3-\bar{e}_3\bar{p}_3\right)+\bar{e}_2\left(\bar{p}_3\bar{C}_{33}+\bar{e}_3\bar{\beta}_r\right)}{\bar{C}_{33}\bar{\eta}_3+\bar{e}_3^2}\right]$$

$$a_{69}=\frac{\bar{p}_m}{\bar{r}\theta_m}\frac{\bar{e}_2\bar{C}_{33}-\bar{e}_3\bar{C}_{32}}{\bar{C}_{33}\bar{\eta}_3+\bar{e}_3^2}$$

$$a_{81}=D\frac{1+\nu}{\bar{E}_i}\qquad a_{8\ \bar{2}}=-\ D\frac{h}{L}-\qquad a_{83}=-D\frac{h}{R}\frac{\bar{p}_m}{\bar{r}\theta_m}$$

$$a_{84}=D\frac{h}{R}\frac{1}{\bar{r}}$$

Where $D=\frac{1}{1-\nu}\frac{\alpha_o^2 Y_o T_o\bar{E}\bar{\alpha}}{\rho_o c_o}\left(\frac{\partial}{\partial\bar{t}}+\bar{\tau}_0\frac{\partial^2}{\partial\bar{t}^2}\right)$

$$a_{87}=\bar{k}\left[\left(\frac{R}{L}\bar{p}_n\right)^2+\left(\frac{\bar{p}_m}{\bar{r}\theta_m}\right)^2\right]+$$

$$\left[\left[\overline{c\rho}+\frac{1+\nu}{(1+\nu)(1-2\nu)}\frac{\alpha_o^2 Y_o T_o\bar{E}_i\bar{\alpha}_i}{\rho_o c_o}\right]\left(\frac{\partial}{\partial\bar{t}}+\bar{\tau}_0\frac{\partial^2}{\partial\bar{t}^2}\right)\right.$$

$$a_{95}=\frac{R}{L}\frac{\bar{P}_n\bar{e}_5}{\bar{C}_{55}}$$

$$a_{96}=\frac{\bar{P}_m\bar{e}_4}{\bar{r}\theta_m\bar{C}_{44}}$$

$$a_{910}=-\frac{h}{R}\frac{\bar{p}_m^2}{\bar{r}^2\theta_m^2}\left(\bar{\eta}_2+\frac{\bar{e}_4^2}{\bar{C}_{44}}\right)-\frac{hR}{L^2}\bar{P}_n^2\left(\bar{\eta}_1+\frac{\bar{e}_5^2}{\bar{C}_{55}}\right)$$

$$a_{101}=\frac{R}{h}\frac{\bar{e}_3}{\bar{C}_{33}\bar{\eta}_3+\bar{e}_3^2}$$

$F_a=\left[F_{ij}\right]$ i = 1-3 , j = 1-6

Where

$$F_{11}=\frac{\bar{C}_{13}\bar{\eta}_3+\bar{e}_1\bar{e}_3}{\bar{C}_{33}\bar{\eta}_3+\bar{e}_3^2}$$

$$F_{12}=\frac{h}{L}\bar{p}_n\left(-\bar{C}_{11}+\frac{\bar{C}_{13}\left(\bar{C}_{13}\bar{\eta}_3+\bar{e}_1\bar{e}_3\right)+\bar{e}_1\left(\bar{e}_3\bar{C}_{13}-\bar{e}_1\bar{C}_{33}\right)}{\bar{C}_{33}\bar{\eta}_3+\bar{e}_3^2}\right)$$

$$F_{13}=\frac{h}{R}\frac{\bar{p}_m}{\theta_m}\left(-\bar{C}_{12}+\frac{\bar{C}_{13}\left(\bar{C}_{23}\bar{\eta}_3+\bar{e}_2\bar{e}_3\right)+\bar{e}_1\left(\bar{e}_3\bar{C}_{23}-\bar{e}_2\bar{C}_{33}\right)}{\bar{C}_{33}\bar{\eta}_3+\bar{e}_3^2}\right)$$

$$F_{14}=\frac{h}{R}\left(\bar{C}_{12}+\frac{\bar{e}_1\left(\bar{C}_{33}\bar{e}_2-\bar{C}_{32}\bar{e}_3\right)-\bar{C}_{13}\left(\bar{e}_2\bar{e}_3+\bar{C}_{32}\bar{\eta}_3\right)}{\bar{C}_{33}\bar{\eta}_3+\bar{e}_3^2}\right)$$

$$F_{15}=-\bar{\beta}_z+\frac{\bar{C}_{13}\left(\bar{\beta}_z\bar{\eta}_3-\bar{e}_3\bar{p}_3\right)+\bar{e}_1\left(\bar{p}_3\bar{C}_{33}+\bar{e}_3\bar{\beta}_z\right)}{\bar{C}_{33}\bar{\eta}_3+\bar{e}_3^2}$$

$$F_{16}=\frac{\bar{C}_{13}\bar{e}_3-\bar{e}_1\bar{C}_{33}}{\bar{C}_{33}\bar{\eta}_3+\bar{e}_3^2}$$

$$F_{21}=\frac{\bar{C}_{23}\bar{\eta}_3+\bar{e}_2\bar{e}_3}{\bar{C}_{33}\bar{\eta}_3+\bar{e}_3^2}$$

$$F_{22}=\frac{h}{L}\bar{p}_n\left(-\bar{C}_{12}+\frac{\bar{C}_{23}\left(\bar{C}_{13}\bar{\eta}_3+\bar{e}_1\bar{e}_3\right)+\bar{e}_2\left(\bar{e}_3\bar{C}_{13}-\bar{e}_1\bar{C}_{33}\right)}{\bar{C}_{33}\bar{\eta}_3+\bar{e}_3^2}\right)$$

$$F_{23}=\frac{h}{R}\frac{\bar{p}_m}{\theta_m}\left(-\bar{C}_{22}+\frac{\bar{C}_{23}\left(\bar{C}_{23}\bar{\eta}_3+\bar{e}_2\bar{e}_3\right)+\bar{e}_2\left(\bar{e}_3\bar{C}_{23}-\bar{e}_2\bar{C}_{33}\right)}{\bar{C}_{33}\bar{\eta}_3+\bar{e}_3^2}\right)$$

$$F_{24}=\frac{h}{R}\left(\bar{C}_{22}+\frac{\bar{e}_2\left(\bar{C}_{33}\bar{e}_2-\bar{C}_{32}\bar{e}_3\right)-\bar{C}_{23}\left(\bar{e}_2\bar{e}_3+\bar{C}_{32}\bar{\eta}_3\right)}{\bar{C}_{33}\bar{\eta}_3+\bar{e}_3^2}\right)$$

$$F_{25} = -\bar{\beta}_0 + \frac{\bar{C}_{23}\left(\bar{\beta}_r\bar{\eta}_3 - \bar{e}_3 p_3\right) + \bar{e}_2\left(\bar{p}_3\bar{C}_{33} + \bar{e}_3\bar{\beta}_r\right)}{\bar{C}_{33}\bar{\eta}_3 + \bar{e}_3^2}$$

$$F_{26} = \frac{\bar{C}_{23}\bar{e}_3 - \bar{e}_2\bar{C}_{33}}{\bar{C}_{33}\bar{\eta}_3 + \bar{e}_3^2} \qquad F_{32} = \bar{C}_{66}\frac{h}{L}\bar{p}_n \qquad F_{33} = \bar{C}_{66}\frac{h}{R}\frac{\bar{p}_m}{\theta_m}$$

$$\hat{G}_f = \bar{G}_f \text{ unless } \frac{\partial}{\partial t} \to S \ , \ \frac{\partial^2}{\partial t^2} \to S^2$$

$$\hat{G}_p = \bar{G}_p \text{ unless } \frac{\partial}{\partial t} \to S \ , \ \frac{\partial^2}{\partial t^2} \to S^2$$

$$I_f(i,j)_{8\times 8} = \left(\frac{\bar{r}_o}{\bar{r}_i + \bar{h}_m}\right)^{m_1} \times I(i,j)_{8\times 8} \quad \text{if } i = 1,5,6$$

else

$$I_f(i,j)_{8\times 8} = I(i,j)_{8\times 8}$$

Where $I(i,j)_{8\times 8}$ is unit matrix

## Disclosure of Potential Conflicts of Interest

The Authors declare that there is no conflict of interest

## Reference


[1] Ootao Y, Tanigawa Y. Three-dimensional transient piezo-thermo-elasticity in functionally graded rectangular plate bonded to a piezoelectric layer. Int. J. of Solids and Structures 2000; 37: 4377-4401.

[2] Cho H, Kardomateas Thermal shock stresses due to heat convection at a bounding surface in a thick orthotropic cylindrical shell. International Journal of Solids and Structures 2001; 38: 2769-2788.

[3] Liew KM, He XQ, Ng TY, Sivashanker S. Finite element piezo-thermo-elasticity analysis and the active control of FGM plates with integrated piezoelectric sensors and actuators. Computational Mechanics 2003; 31: 350-358.

[4] Ding HJ, Wang HM, Chen WQ. A solution of a non-homogeneous orthotropic cylindrical shell for axisymmetric plane strain dynamic thermoelastic problems. Journal of Sound and Vibration 2003; 263: 815–829

[5] Dai HL, Wang X. Stress wave propagation in laminated piezoelectric spherical shells under thermal shock and electric excitation. European Journal of Mechanics A/Solids 2005; 24: 263–276.

[6] Dai HL, Wang X. Thermo-electro-elastic transient responses in piezoelectric hollow structures. International Journal of Solids and Structures 2005; 42: 1151–1171.

[7] Oh IK. Thermo-piezo-elastic nonlinear dynamics of active piezolaminated plates. Smart Mater. Struct. 2005; 14: 823-834.

[8] Huang XL, Shen HS. Vibration and dynamic response of functionally graded plates with piezoelectric actuators in thermal environment . Journal of Sound and Vibration 2006; 289: 25-53.

[9] Giannopoulos G, Vantomme J. A thermal–electrical–mechanical coupled FE formulation using discrete layer kinematics for the dynamic analysis of smart plates. Smart Mater. Struct. 2006; 15: 1846-1857.

[10] Li XY, Ding HJ, Chen WQ. Three-dimensional analytical solution for functionally graded magneto–electro-elastic circular plates subjected to uniform load. Comps Struct. 2008; 83: 381-390.

[11] Farzad Ebrahimi , Abbas Rastgoo, An analytical study on the free vibration of smart circular thin FGM plate based on classical plate theory, Thin Walled Structures 2008; 46: 1402-1408.

[12] Farzad Ebrahimi , Abbas Rastgoo, An analytical study on the free vibration of smart circular thin FGM plate based on classical plate theory, Smart Materials and Structures 2008; 17: 17015044.

[13] Farzad Ebrahimi , Abbas Rastgoo, M.K. Kargarnovin, Analytical investigation on axisymmetric free vibrations of moderately thick circular functionally graded plate integrated with piezoelectric layers, Journal of Mechanical Science and Technology 2008; 22: 1058-1072.

[14] Kar A, Kanoria M. Generalized thermoelastic functionally graded orthotropic hollow sphere under thermal shock with three-phase-lag effect. European Journal of Mechanics A/Solids 2009; 28: 757–767.

[15] Farzad Ebrahimi , Abbas Rastgoo, M.K. Kargarnovin, Analytical investigation on axisymmetric free vibrations of moderately thick circular functionally graded plate integrated with piezoelectric layers, Journal of Mechanical Science and Technology 2008; 22: 1058-1073.

[16] F. Ebrahim, M.H. Naei, A. Rastgoo, Geometrically nonlinear vibration analysis of piezoelectrically

actuated FGM plate with an initial large deformation , Journal of Mechanical Science and Technology 2009; 23: 2107-2124.

[17] Alibeigloo A. Thermo-elasticity solution of functionally graded plates integrated with piezoelectric sensor and actuator layers. Journal of Thermal Stresses 2010; 33: 754-774.

[18] Ying J, Wang HM. Axisymmetric thermoelastic analysis in a finite hollow cylinder due to nonuniform thermal shock. International Journal of Pressure Vessels and Piping 2010; 87: 714-720.

[19] Chitikireddy R, Datta SK, Shah AH, Bai H. Transient thermoelastic waves in an anisotropic hollow cylinder due to localized heating . International Journal of Solids and Structures 2011; 48: 3063–3074.

[20] Alibeigloo A. Exact solution of an FGM cylindrical panel integrated with sensor and actuator layers under thermomechanical load. Smart Mater. Struct. 2011; 20: 035002 (14pp).

[21] F. Ebrahim, Analytical Investigation on Vibrations and Dynamic Response of Functionally Graded Plate Integrated with Piezoelectric Layers in Thermal Environment , Mechanics of Advanced Materials and Structures 2013; 20: 854-870.

[22] Asemi K , Salehi M, Mehdi Akhlaghi M. Transient thermal stresses in functionally graded thick truncated cones by graded finite element method. International Journal of Pressure Vessels and Piping 2014; 119: 52-61.

[23] Shao XS, Fu Y, Chen Y. Nonlinear dynamic response and active control of fiber metal laminated plates with piezoelectric actuators and sensors in unsteady temperature field. Smart Mater. Struct. 2015; 24: 055023(11pp).

[24] Zenkour AM. Three-dimensional thermal shock plate problem within the framework of different thermo-elasticity . Composite Structures 2015; 132:1029-1042.

[25] Liang X, Kou HI, Wang L, Palmer AC, Wang Z, Liu G. Three-dimensional transient analysis of functionally graded material annular sector plate under various boundary conditions . Composite Structures 2015; 132:584-596.

[26] Duc ND, Cong PH, Quang VD. Nonlinear dynamic and vibration analysis of piezoelectric eccentrically stiffened FGM plates in thermal environment. International Journal of Mechanical Sciences 2016; 115-116: 711-722.

[27] Wang YZ, Liu D, Wang Q, Zhou JZ. Asymptotic analysis of thermoelastic response in functionally graded thin plate subjected to a transient thermal shock. Composite Structures 2016;139: 233-242.

[28] Pandey S, Pradyumna S. A finite element formulation for thermally induced vibrations of functionally graded material sandwich plates and shell panels. Composite Structures 2017;160: 877-886.

[29] Jafarnezhad MR, Eslami MR. Coupled thermoelasticity of FGM annular plate under lateral thermal shock. Composite structures 2017; 168: 758-771 .

[30] Alibeigloo A. Three dimensional coupled thermoelasticity solution of sandwich plate with FGM core under thermal shock. Composite Structures 2017; 177: 96-103.